



Article

Biological Activity of Novel Organotin Compounds with a Schiff Base Containing an Antioxidant Fragment

Taisiya A. Antonenko¹, Yulia A. Gracheva¹, Dmitry B. Shpakovsky¹, Mstislav A. Vorobyev², Dmitrii M. Mazur¹ , Victor A. Tafeenko¹, Yury F. Oprunenko¹, Elena F. Shevtsova³ , Pavel N. Shevtsov³, Alexey A. Nazarov^{1,*} and Elena R. Milaeva¹

¹ Department of Chemistry, M. V. Lomonosov Moscow State University, Leninskie Gory 1/3, 119991 Moscow, Russia

² Institute of Geography of the Russian Academy of Sciences, Department of Glaciology, 117312 Moscow, Russia

³ Institute of Physiologically Active Compounds of Russian Academy of Sciences, 142432 Chernogolovka, Russia

* Correspondence: nazarov@med.chem.msu.ru

Abstract: A series of novel organotin(IV) complexes on the base of 2-(N-3',5'-di-*tert*-butyl-4'-hydroxyphenyl)-iminomethylphenol (L) of formulae $\text{Me}_2\text{SnBr}_2(\text{L})_2$ (1), $\text{Bu}_2\text{SnCl}_2(\text{L})_2$ (2), $\text{Ph}_2\text{SnCl}_2(\text{L})$ (3), $\text{Ph}_2\text{SnCl}_2(\text{L})_2$ (4) $\text{Ph}_3\text{SnBr}(\text{L})_2$ (5) were synthesized and characterized by ¹H, ¹³C, ¹¹⁹Sn NMR, IR, ESI-MS and elemental analysis. The crystal structures of initial L and complex 2 were determined by XRD method. It was found that L crystallizes in the orthorhombic syngony. The distorted octahedron geometry around Sn center is observed in the structure of complex 2. Intra- and inter-molecular hydrogen bonds were found in both structures. The antioxidant activity of new complexes as reducing agents, radical scavengers and lipoxygenase inhibitors was estimated spectrophotometrically in CUPRAC and DPPH tests (compounds 1 and 5 were found to be the most active in both methods), and in the process of enzymatic oxidation in vitro of linoleic acid under the action of lipoxygenase LOX 1-B ($\text{EC}_{50} > 33.3 \mu\text{M}$ for complex 2). Furthermore, compounds 1–5 have been investigated for their antiproliferative activity in vitro towards HCT-116, MCF-7 and A-549 and non-malignant WI-38 human cell lines. Complexes 2 and 5 demonstrated the highest activity. The plausible mechanisms of the antiproliferative activity of compounds, including the influence on the polymerization of Tb+MAP, are discussed. Some of the synthesized compounds have also actively induced apoptosis and blocked proliferation in the cell cycle G2/M phase.

Keywords: organotin complexes; Schiff base; antioxidant activity; antiproliferative activity; apoptosis; cell cycle



Citation: Antonenko, T.A.; Gracheva, Y.A.; Shpakovsky, D.B.; Vorobyev, M.A.; Mazur, D.M.; Tafeenko, V.A.; Oprunenko, Y.F.; Shevtsova, E.F.; Shevtsov, P.N.; Nazarov, A.A.; et al. Biological Activity of Novel Organotin Compounds with a Schiff Base Containing an Antioxidant Fragment. *Int. J. Mol. Sci.* **2023**, *24*, 2024. <https://doi.org/10.3390/ijms24032024>

Academic Editor: Antonio Lucacchini

Received: 28 December 2022

Revised: 16 January 2023

Accepted: 17 January 2023

Published: 19 January 2023



Copyright: © 2023 by the authors. Licensee MDPI, Basel, Switzerland. This article is an open access article distributed under the terms and conditions of the Creative Commons Attribution (CC BY) license (<https://creativecommons.org/licenses/by/4.0/>).

1. Introduction

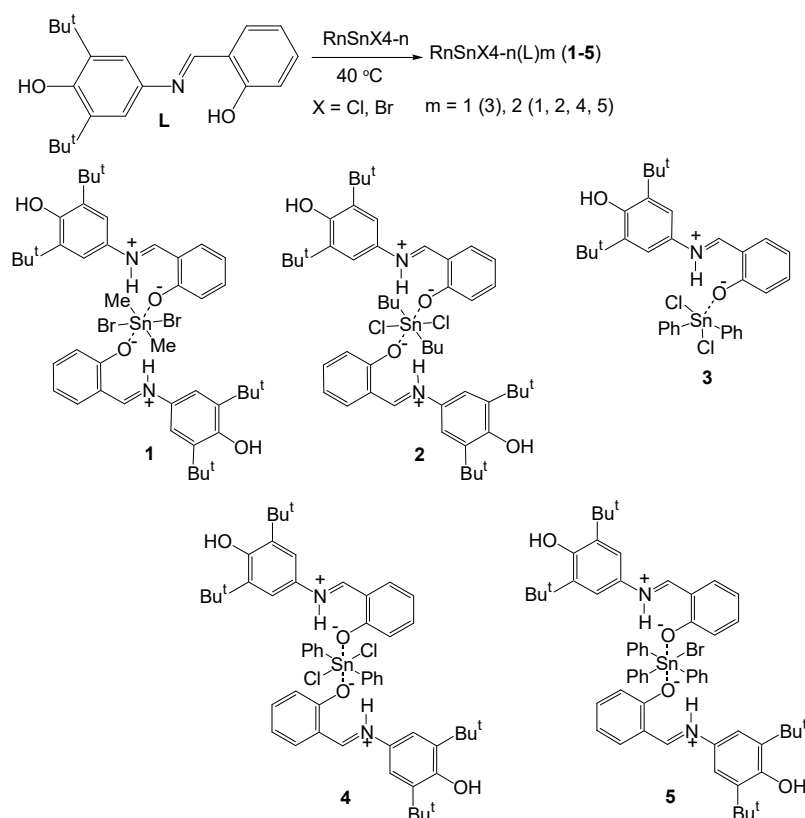
It is known that platinum compounds were the first drugs based on metal compounds that were widely used in cancer treatment therapy. Nevertheless, they are highly toxic and show poor selectivity for different cell lines, and many types of cancer have developed resistance to them. Therefore, the search for new organometallic compounds with anti-tumor activity is an urgent task [1–3]. A significant part of this large class of compounds is represented by organotin complexes. It is known that tin complexes with coordination number >4 have a wide spectrum of biological activity, such as fungicidal, antibacterial, nematocidal, insecticidal, herbicidal, anti-inflammatory and anti-tumor activities [4]. It was found that the structure of anti-tumor drugs based on tin compounds is characterized by the presence of a stable ligand-metal bond resistant to hydrolysis. Higher cytotoxicity is manifested when the coordination environment of the tin atom is completely filled (CN = 6) and when the Sn–N and Sn–S bonds are the shortest [5].

Schiff bases common organic ligands. They can be applied as dyes, catalysts, intermediates, polymer stabilizers and pigments. These compounds also demonstrate

various types of biological activities, e.g., antimalarial, anti-inflammatory, antiviral and antiproliferative ones [6]. Complexes of Fe(III), Co(II), Zn(II), and Zr(IV) with Schiff base gemifloxacin exhibited promising antifungal activity [7]. Also, there is a study reporting significant biological activity of enrofloxacin Schiff base complexes (H_2Er_x-en) of Fe(III), Y(III), Zr(IV) and La(III) that demonstrated extremely significant antibacterial activity data [8]. The Cu (II) complex with Gat-o-phdn Schiff base (4E,4'E)-4,4'-(1,2-phenylenebis (azaneylylidene))bis(1-cyclopropyl-6-fluoro-8-methoxy-7-(3-methylpiperazin-1-yl)-1,4-dihydroquinoline-3-carboxylic acid demonstrated very high antimicrobial activity against *Staphylococcus aureus* [9].

One of the proposed mechanisms of organotin's action may be due to Sn atom's ability to bind to sulfhydryl groups, followed by DNA destruction that ultimately leads to cell death [10]. The toxicity of organotin can also induce oxidative stress in living organisms. To decrease their unwanted high toxicity, it is proposed to use antioxidants; 2,6-dialkylphenols are known to be vitamin E mimetics and inhibitors of radical oxidative processes [11,12]. We found previously that organotin complexes containing Schiff base with 2,6-dialkylphenol fragment demonstrate both good antioxidant and cytotoxic activities [13].

The purpose of this work was the synthesis of novel organotin complexes 1–5 with Schiff base L containing an antioxidant fragment of 2,6-di-*tert*-butylphenol (Scheme 1) and the study of their biological activity. Herein we report the antioxidant and antiproliferative properties of new complexes 1–5.



Scheme 1. Synthesis of organotin complexes 1–5 based on L.

2. Results and Discussion

2.1. Synthesis and Characterization

Novel complexes 1–4 were obtained by the interaction of L with organotin chlorides Bu_2SnCl_2 , Ph_2SnCl_2 and bromide Me_2SnBr_2 (Scheme 1) in methylene chloride with stirring and low heating ($40\text{ }^\circ\text{C}$). The new complex 5 (Scheme 1) was synthesized by the interaction of L with Ph_3SnBr in a mixture of chloroform and ethanol. Compounds 1–5 were

found to be stable in air and were explored by elemental analysis, IR, ^1H , ^{13}C and ^{119}Sn NMR spectroscopy.

The IR, ^1H and ^{13}C spectroscopic data (Figures S1–S10) are comparable with those for structurally similar complexes [13]. The IR spectra of compounds 1–5 demonstrate absorption bands in the region of $3492\text{--}3643\text{ cm}^{-1}$, appropriating to the stretching vibrations of the O–H bond of the sterically hindered non-associated phenolic group.

The proton signal of the phenol group is absent in the ^1H NMR spectra of complexes 1–5, whereas for the starting compound L the signal is observed at 13.64 ppm due to solvent exchange. The spin-spin interaction of H–Sn (Ph_2Sn fragment, $^2J_{\text{Sn-H}} = 80\text{ Hz}$) is also found in the ^1H NMR spectrum of complex 4.

The chemical shifts in ^{119}Sn spectra varied in the wide interval (from -326 to $+112\text{ ppm}$) depending on the environment of Sn atom (Figures S11–S15).

Compounds 1–5 were also characterized by HRMS. It turns out that during electrospray ionization, the complex structure is broken, and the charge stays on the ligand part only. There is however indirect evidence, which is described below, in favor of the proposed structure coming from HRMS data. It appears that some intermolecular reactions or redox reactions besides just ionization processes may take place during ESI. The ligand environment, hence, could be significantly changed through the loss of some ligands or by substitution reactions. Compound 1 forms ions m/z 326.2101 $\text{C}_{21}\text{H}_{28}\text{O}_2\text{N}$, m/z 474.1431 $\text{C}_{23}\text{H}_{32}\text{O}_2\text{NSn}$ (Me_2SnL), m/z 799.3463 $\text{C}_{44}\text{H}_{59}\text{O}_4\text{N}_2\text{Sn}$ (Me_2SnL_2) (Figure 1). Base peak m/z 326.2104 ($\text{C}_{21}\text{H}_{28}\text{O}_2\text{N}$) corresponds to the protonated molecule of ligand.

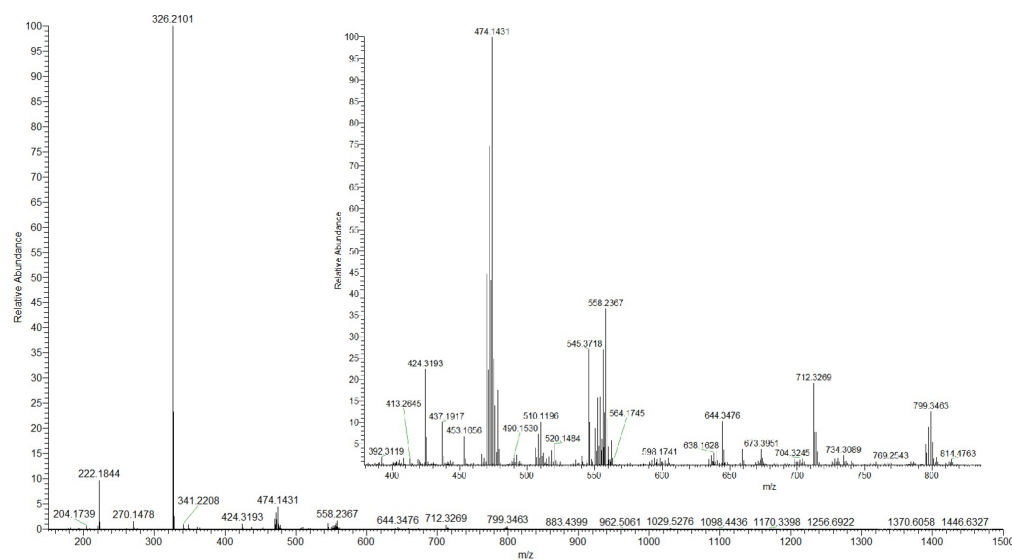


Figure 1. ESI mass spectrum of compound 1.

Similar ions are observed in the mass spectrum of compound 2 with m/z 326.2101 $\text{C}_{21}\text{H}_{28}\text{O}_2\text{N}$ (L), m/z 558.2370 $\text{C}_{29}\text{H}_{44}\text{O}_2\text{NSn}$ (Bu_2SnL), m/z 594.2129 $\text{C}_{29}\text{H}_{45}\text{O}_2\text{NClSn}$ (Bu_2SnClL), m/z 883.4399 $\text{C}_{50}\text{H}_{71}\text{O}_4\text{N}_2\text{Sn}$ (Bu_2SnL_2) (Figure S16).

In the case of compound 3 two clusters of ions are observed at m/z 594–602 and m/z 672–680, which the isotopic distribution and accurate masses of which nicely fit the formulae. $\text{C}_{33}\text{H}_{36}\text{O}_2\text{NSn}$ (Ph_2SnL) and $\text{C}_{39}\text{H}_{42}\text{O}_2\text{NSn}$ (Ph_3SnL) correspondingly, result from loss of chloride ligands. Signals of low abundance within m/z 612–636 were assigned for $\text{C}_{33}\text{H}_{37}\text{O}_2\text{NClSn}$ (Ph_2SnClL) and $\text{C}_{33}\text{H}_{38}\text{O}_3\text{NSn}$ (Ph_2SnOHL) (Figure S17).

The base peak in the mass spectrum of compound 4 is similar to that for 3 since they both have the same ligand (Figure S18). However, together with the ions mentioned above there are signals in the m/z 800–950 range (e.g., m/z 923.3742 corresponding to Ph_2SnL_2 , i.e., $\text{C}_{54}\text{H}_{63}\text{O}_4\text{N}_2\text{Sn}$) bringing evidence to the *bis*-ligand nature of the compound 4. Substitution of Cl-ligands for Br doesn't significantly change the mass spectrum of compound 5 (Figure S19). The most abundant peaks are the same. The bromine

atom is missing in observed signals, but all the rest of the moieties are revealed: m/z 598.1732 $C_{33}H_{36}O_2NSn$ (Ph_2SnL), m/z 676.2203 $C_{39}H_{42}O_2NSn$ (Ph_3SnL), m/z 854.4114 $C_{48}H_{66}O_4N_2Sn$, m/z 923.3744 $C_{54}H_{63}O_4N_2Sn$ (Ph_2SnL_2). Though the studied complexes did not form any molecular species ($[M+H]^+$, $[M+Na]^+$, etc.) under ESI conditions, the ions described above still are useful and reveal the proposed molecular structure.

2.2. Crystal Structures

Recrystallization of compound **L** from a mixture of petroleum ether and CH_2Cl_2 gave orange crystals, which were used for crystallographic analysis (Table 1).

Table 1. Crystal data and the structure refinement details for compounds **L** and **2**.

Compound	L	2
Empirical formula	$C_{21}H_{27}NO_2$	$C_{25}H_{36}ClNO_2Sn_{0.50}$
Fw	325.43	477.33
T, K	293(2)	293(2)
Space group	$P2_12_12_1$	$P2_1/n$
Syngony	Orthorhombic	Monoclinic
a (Å)	6.0356(4)	9.5216(5)
b (Å)	17.5484(14)	11.7902(7)
c (Å)	17.7780(12)	22.4464(11)
α (°)	90.00	90.00
β (°)	90.00	98.820(3)
γ (°)	90.00	90.00
V (Å ³)	1883.0(2)	2490.1(2)
Z	4	4
λ	MoK α	CuK α
$\Delta\rho_{max}/\Delta\rho_{min}$ ($e/\text{Å}^3$)	0.212/−0.210	2.028/−1.732
μ (mm^{-1})	0.073	5.396
GOOF	0.864	1.122
R_1/wR_2 ($I \geq 2\sigma(I)$)	0.0458/0.1172	0.0772/0.2112

It has been established that the ligand crystallizes in the orthorhombic syngony. The N1-C7 bond distance is 1.272(3) Å. X-ray diffraction analysis (XRD) showed the presence of an intramolecular hydrogen bond $O2-H32 \cdots N1$ ($H32 \cdots N1 = 1.47$ Å, $O2-H32 \cdots N1 = 2.54$ Å, angle $O2-H32-N1 = 150.95^\circ$), as well as an intermolecular hydrogen bond $O1-H31 \cdots O2$ ($H31 \cdots O2 = 2.13$ Å, $O1-H31 \cdots O2 = 2.80$ Å, angle $O1-H31-O2 = 137.23^\circ$).

The angle between the ring plane of the 2,6-di-*tert*-butylphenol fragment (C1C2C3C4C5C6) and the ring plane of the unhindered phenol group (C8C9C10C11C12C13) is 22.26° . The molecular structure of the compound is shown in Figure 2. Table 2 demonstrates the individual bond distances and angles of **L**.

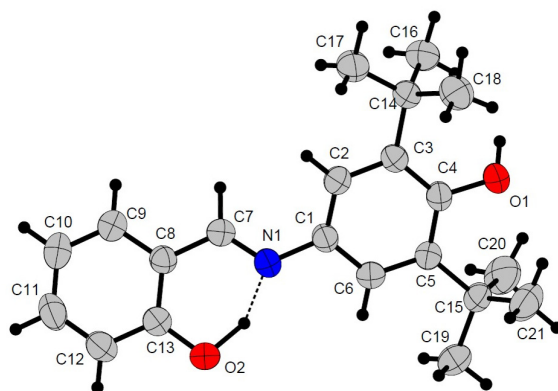
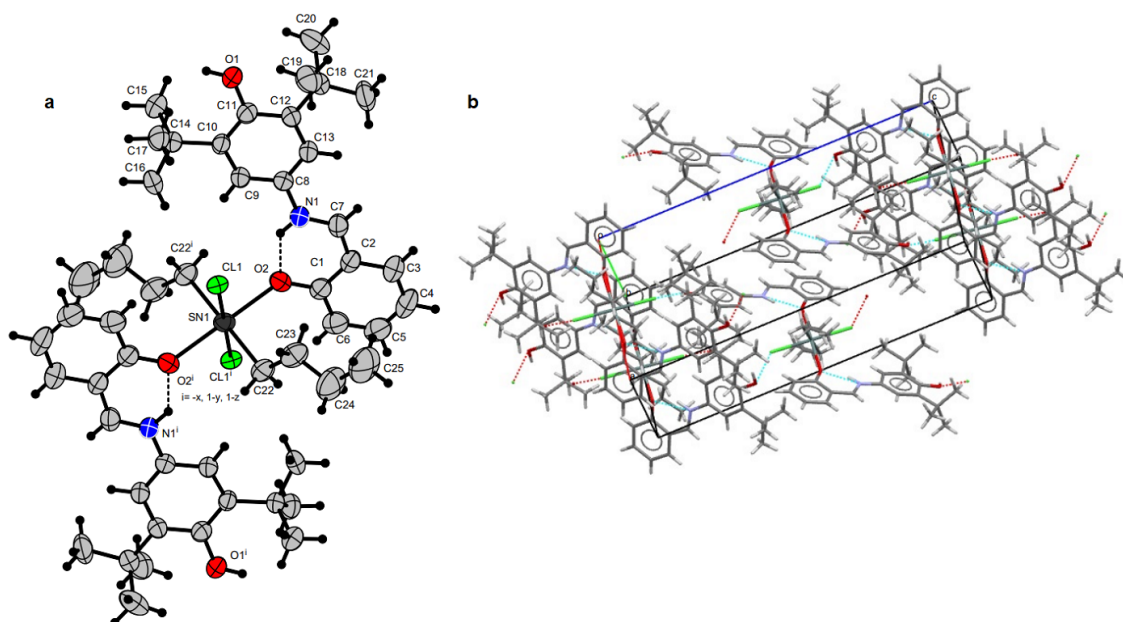


Figure 2. Molecular structure of starting compound **L**.

Table 2. Selected bond distances (Å) and angles (°) for compounds **L** and **2**. Symmetry operation $i = -x, 1 - y, 1 - z$.

L		2	
Selected bond distances (Å)			
O(1)-C(4)	1.365(3)	Sn(1)-C(22)	2.140(7)
O(2)-C(13)	1.342(3)	Sn(1)-O(2)	2.258(4)
N(1)-C(7)	1.272(3)	Sn(1)-Cl(1)	2.6123(18)
N(1)-C(1)	1.419(3)		
Angles (°)			
C(4)-O(1)-H(31)	113(2)	C(22)-Sn(1)-O(2)	88.31(19)
C(13)-O(2)-H(32)	103.9(17)	C(22) ⁱ -Sn(1)-O(2)	91.69(19)
C(7)-N(1)-C(1)	123.4(2)	C(22)-Sn(1)-O(2) ⁱ	91.69(19)
C(7)-N(1)-H(32)	101.4(14)	C(22) ⁱ -Sn(1)-O(2) ⁱ	88.31(19)
C(1)-N(1)-H(32)	134.8(14)	O(2)-Sn(1)-O(2) ⁱ	180.00(18)
C(6)-C(1)-N(1)	116.1(2)	C(22)-Sn(1)-Cl(1)	91.89(15)
C(2)-C(1)-N(1)	124.5(2)	C(22) ⁱ -Sn(1)-Cl(1)	88.11(15)
O(1)-C(4)-C(5)	115.2(2)	O(2)-Sn(1)-Cl(1)	92.11(12)
O(1)-C(4)-C(3)	122.6(2)	O(2) ⁱ -Sn(1)-Cl(1)	87.89(12)
N(1)-C(7)-C(8)	121.8(2)	C(22)-Sn(1)-Cl(1) ⁱ	88.11(15)
N(1)-C(7)-H(7)	124.3(14)	C(22) ⁱ -Sn(1)-Cl(1) ⁱ	91.89(15)
O(2)-C(13)-C(12)	119.6(2)	O(2)-Sn(1)-Cl(1) ⁱ	87.89(12)
O(2)-C(13)-C(8)	120.5(2)	O(2) ⁱ -Sn(1)-Cl(1) ⁱ	92.11(12)

As a result of the recrystallization of compound **2** from hexane, orange single crystals, suitable for XRD, were obtained. The coordination number around the tin atom in crystals (L)₂Bu₂SnCl₂ (**2**) is 6; the coordination polyhedron is a distorted octahedron. The butyl groups, chlorine atoms, and oxygen atoms of the unhindered phenolic group are in a trans-position with respect to each other in the inner coordination sphere of the tin atom (Figure 3a).

**Figure 3.** Molecular structure of **2** (a); hydrogen bonds in crystal packing **2** (b).

Due to proton transfer from the oxygen atom O2 to the nitrogen atom N1, intramolecular hydrogen bonds N1-H21...O2 are formed in the structure (H21...O2 = 1.80 Å, N1-H21...O2 = 2.58 Å, angle N1-H21-O2 = 137.85°) (Figure 3b). It should be noted that, in comparison with the initial ligand, in the structure of the obtained complex, the angle between the ring plane of the 2,6-di-*tert*-butylphenol fragment and the ring plane of the

unhindered phenol group in the structure of **2** decreases significantly and amounts to 4.50° , i.e., these fragments lie almost in the same plane. The individual bond distances and angles of **2** are listed in Table 2.

2.3. CUPRAC Assay (Cu^{2+} Reducing)

One of the methods for studying the antioxidant activity of compounds is to research their ability to one-electron reduction using the spectrophotometric CUPRAC test. Neocuproine (2,9-dimethyl-1,10-phenanthroline) forms a complex with Cu^+ in the presence of antioxidants with an absorption maximum at 450 nm [14]. The experiment was carried out to increase the optical density of a solution of the complex in ethanol. Trolox (6-hydroxy-2,5,7,8-tetramethylchroman-2-carboxylic acid) was used as a standard. The results are presented as TEAC values (Trolox equivalents antioxidant capacity, Table 3). TEAC for Trolox is 1.00 ± 0.03 . It was shown that among the most active complexes are compounds **1**, **2**, **4** and **5**.

Table 3. The TEAC values of Cu^{2+} reducing activity in CUPRAC test for compounds **L**, **1**–**5**.

Compound	TEAC (CUPRAC)
L	0.81 ± 0.03 [13]
1	3.37 ± 0.03
2	2.78 ± 0.04
3	1.19 ± 0.09
4	2.64 ± 0.07
5	2.31 ± 0.06

Results presented as mean \pm SD obtained using data from at least three independent experiments.

2.4. DPPH Radical Scavenging Activity

A method for studying the antioxidant (radical scavenging) activity of compounds is their ability to reduce the stable 2,2-diphenyl-1-picrylhydrazyl (DPPH) radical by hydrogen atom transfer [15].

The activity of tin compounds **1**–**5** in the DPPH test, as well as the initial ligand **L**, was studied spectrophotometrically by measuring the decrease in the optical density of DPPH at a wavelength of 517 nm for 1 h. The value of the EC_{50} parameter (the effective concentration of the compound required to reduce the concentration of the DPPH radical by 50%) was determined graphically according to the dependence of the content of the remaining DPPH (in %) on the primary concentration of compounds (0.01–0.1 mM). EC_{50} values are presented in Table 4.

Table 4. EC_{50} and k values in the DPPH test (EtOH, 20°C) in the presence of **1**–**5**.

Compound	1	2	3	4	5	
EC_{50} , μM	16 ± 2	20 ± 3	30 ± 3	19 ± 2	23 ± 2	
s	0.32	0.4	0.30	0.38	0.23	
s^{-1}	3.13	2.5	3.36	2.60	4.32	
k ($\text{L mol}^{-1} \text{s}^{-1}$)						
C	0.06 mM	*	49 ± 5	*	*	
	0.04 mM	31 ± 4	29 ± 3	5 ± 1	49 ± 4	10 ± 1
	0.02 mM	13 ± 4	2 ± 0.5	1 ± 0.2	3 ± 0.5	3 ± 0.4
	0.01 mM	1 ± 0.3	0.7 ± 0.1	0.9 ± 0.1	2 ± 0.1	0.7 ± 0.1

$s = 2 \cdot \text{EC}_{50} / C_0(\text{DPPH})$ —the number of moles of compound required to reduce 1 mole of DPPH; s^{-1} —the number of moles of DPPH reduced by 1 mole of the compound; the initial concentration of DPPH is 0.1 mM. Results presented as mean \pm SD obtained using at least from three independent experiments.*—the parameter is not defined due to the high speed of the reaction.

Since compounds 1–5 showed rather high activity, their reaction kinetics were studied, which corresponds to the second order equation. The rate constants k (for each concentration) are obtained from the plot of $1/[\text{DPPH}]$ vs. time (Table 4). It is known that k for **L** at a concentration of 0.06 mM is $10.9 \text{ L mol}^{-1} \text{ s}^{-1}$ [13]. At concentrations higher than 0.04 mM the rate of the DPPH reduction was too high to be evaluated.

2.5. Lipoxygenase Inhibition Assessment

Lipoxygenase LOX 1-B is a plant enzyme that belongs to the class of iron-containing oxygenases and catalyzes the stereospecific oxidation of polyunsaturated fatty acids in the cell, including linoleic acid. It is known that lipoxygenase is able to participate in the destruction of biomembranes [16]. Therefore, the ability of a compound to inhibit this enzyme may indicate its potential antioxidant and anti-inflammatory properties. The antioxidant properties of the obtained compounds were also evaluated in the process of enzymatic oxidation of linoleic acid under the action of lipoxygenase LOX 1-B in vitro. The experiment was carried out by spectrophotometry measuring the content of the oxidation product of linoleic acid—the corresponding hydroperoxides at λ_{max} 234 nm. It was found that the majority of the compounds promote the oxidation of linoleic acid, while complex **2** is only a moderate inhibitor of lipoxygenase ($\text{EC}_{50} > 33.3 \text{ }\mu\text{M}$). The results are listed in Table 5.

Table 5. EC_{50} (μM) and degree of inhibition (I, %) of LOX 1-B lipoxygenase in the presence of compound **2**.

C, μM	I, %
0.8	22.66
8.3	27.59
16.6	31.21
33.3	39.55

2.6. Antiproliferative Activity

The antiproliferative activity of compounds 1–5 was also studied. The compounds were investigated against HCT-116 (human colon cancer), MCF-7 (human breast cancer), A-549 (adenocarcinoma human alveolar basal epithelial) and WI-38 (diploid human cell line composed of fibroblasts) cells using the MTT test [17]. The IC_{50} values were determined in comparison with cisplatin (Table 6).

Table 6. IC_{50} values (μM) against HCT-116, MCF-7, A-549 and WI-38 cell lines for compounds 1–5 and cisplatin.

Compound	IC_{50} , μM			
	HCT-116	MCF-7	A-549	WI-38
1	58.2 ± 14	80.6 ± 6	89 ± 17	58.2 ± 8
2	1.6 ± 0.2	4.3 ± 0.5	5.7 ± 1	1.6 ± 0.2
3	3.8 ± 0.5	6.3 ± 0.7	7.7 ± 1.4	2.3 ± 0.3
4	3.1 ± 0.4	5.1 ± 0.6	6.8 ± 1.8	2.1 ± 0.3
5	0.32 ± 0.08	0.29 ± 0.03	0.30 ± 0.04	0.2 ± 0.05
cisplatin	9.04 ± 0.7	11 ± 1	16.7 ± 3	4.8 ± 0.5

Results presented as mean \pm SD obtained using at least from three independent experiments.

It is known that, depending on the organic substituent nature, the cytotoxicity of organotin compounds $\text{R}_n\text{SnX}_{4-n}\text{L}$ decreases in accordance with $n\text{-Bu} > \text{Ph}, \text{Et} > \text{Me}$ [18,19].

Among the obtained tin complexes, the triphenyltin complex **5** exhibits nanomolar activity (Table 6) that is consistent with the results of our previous works concerning triphenyltin complexes based on 2,6-di-*tert*-butyl-4-mercaptophenol which exhibited the high activity related with the high lipophilicity of Ph_3Sn fragment. In addition, complexes based

on dibutyltin and diphenyltin 2–4 also demonstrate high antiproliferative activity (Figure 4). The activity of obtained complexes against nonmalignant cells WI-38 is comparable to that of HCT-116 cancer cells.

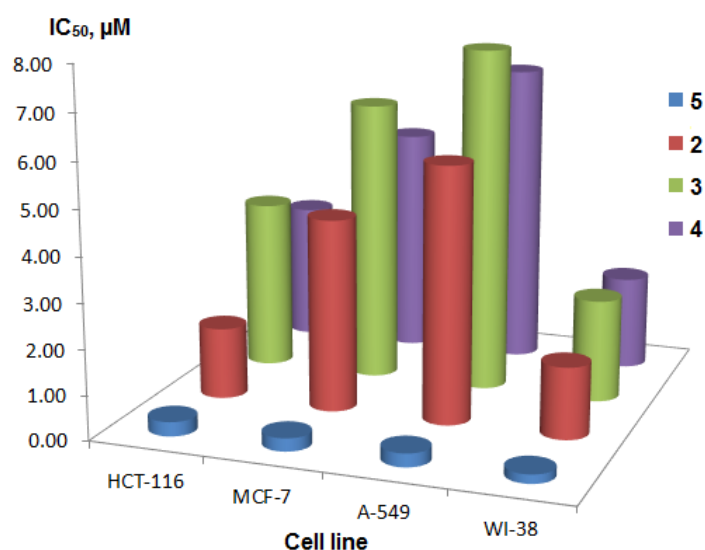


Figure 4. Survival of cell lines HCT-116, MCF-7, A-549 and WI-38 in the presence of compounds 2–5.

2.7. Cell Death and Cell Cycle Analysis

Apoptosis, known as programmed cell death, is a carefully controlled, energy-dependent process. Cells initiate intracellular processes by responding to specific induction signals. This leads to characteristic physiological changes, which include the externalization of phosphatidylserine (PS) to the cell surface. PS is a membrane component that is usually localized on the inside of the cell membrane. At the beginning of the apoptotic pathway, PS molecules move to the outer surface of the cell membrane, where they can easily be bound by annexin V, a calcium-dependent phospholipid-binding protein with a high affinity for PS. To prove the hypothesis that antiproliferative activity correlates with the induction of apoptosis by organotin compounds, we studied the apoptotic profile of selected cancer cells. The mechanism of cell death was monitored as Annexin V/7-AAD reactivity for compounds 2 and 5 in HCT-116 cells using the Muse[®] AnnexinV& Dead Cell Kit (Luminex Corp., Austin, TX, USA) by flow cytometry [20]. Cells were incubated with compounds and cisplatin for 24 and 48 h at concentrations corresponding to 2-IC₅₀ values. Both compounds were shown to induce apoptosis actively. The overall percentage of apoptotic cells is 42.6 and 26.8% for 2 and 5, respectively. Interestingly, for compound 2 the main fraction of cells was found in late apoptosis (32.4%). The percentage of apoptotic cells did not exceed 10.3% in the control group (Figure 5). Thereby, HCT-116 cells turned out to be more sensitive to the action of compound 2 after 24 h of incubation.

An overall increase in apoptotic cells for studied compounds was observed after 48 h, e.g., for 2 their number approaches 65%. The fraction of cells in late apoptosis was 46.3% for 2 (Figure 6).

The cell cycle can be considered the smallest part of the life cycle. It is the series of steps of growth and development that a cell goes through between its birth and reproduction—dividing to form two new daughter cells. For cell division, several tasks must be taken: the cell must grow (G1 phase), copy its genetic material (S phase), prepare to divide (G2 phase), and divide (by mitosis, or M phase).

The assay uses propidium iodide (PI) based staining of DNA content to discriminate and measure the percentage of cells in each cell cycle phase (G0/G1, S, and G2/M). PI discriminates cells at different stages of the cell cycle, based on differential DNA content in the presence of RNase to increase the specificity of DNA staining.

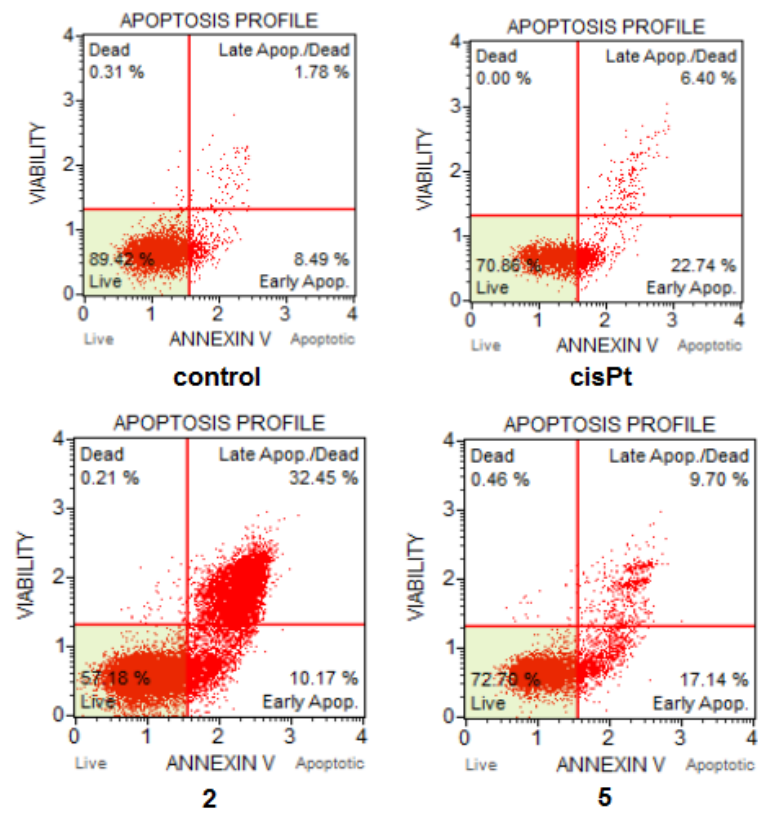


Figure 5. HCT-116 apoptotic profile after treatment with cisplatin and compounds 2, 5 after 24 h. Concentration of compounds 2-IC₅₀ (μM).

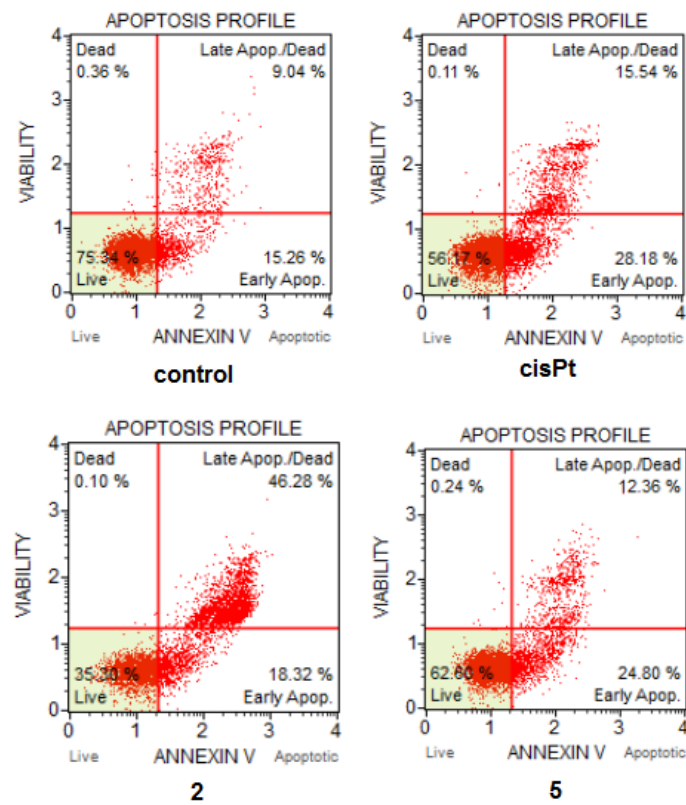


Figure 6. HCT-116 apoptotic profile after treatment with cisplatin and compounds 2, 5 after 48 h. Concentration of compounds 2-IC₅₀ (μM).

The effect of compounds **2** and **5** on cell cycle arrest by flow cytometry was carried out. HCT-116 cells were treated for 24 h with compounds at the concentrations of IC_{50} . It was found that compounds block proliferation in the G2/M phase of the cell cycle, preparation for mitosis-mitosis (Figure 7).

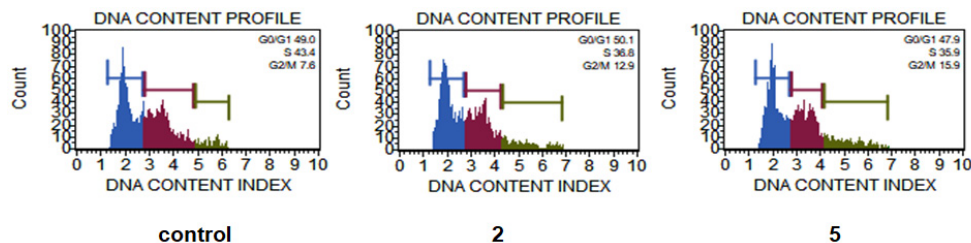


Figure 7. HCT-116 cell cycle analysis after treatment with compounds **2** and **5**. Concentration of compounds IC_{50} (μ M).

2.8. Tubulin Polymerization

It is known that microtubules and their main component tubulin are the prospective targets of antiproliferative chemotherapy drugs. In our previous works [11,21] we demonstrated that cytotoxic organotin complexes containing 2,6-di-*tert*-butylphenol moieties are able to interact with tubulin SH groups. These results suggest that the antiproliferative anti-tumor effects of these compounds may be associated with the disruption of microtubule assembly due to the inhibition of tubulin polymerization in the presence of organotin complexes.

In this work, we studied the influence of the most active compounds **2** and **5** on the crude preparation of Tb+MAP polymerization. It was found that both compounds affect the guanosine triphosphate (GTP) dependent polymerization of Tb+MAP; some stimulation of polymerization is observed for compound **5** and for compound **2** there is a significant blockade of this process that indicates a potential antiproliferative activity (Figure 8). Both stimulation and blockade of the process of tubulin polymerization can be mechanisms of the antiproliferative activity of the compounds, disrupting the dynamic processes of the cell division microtubules spindle [22].

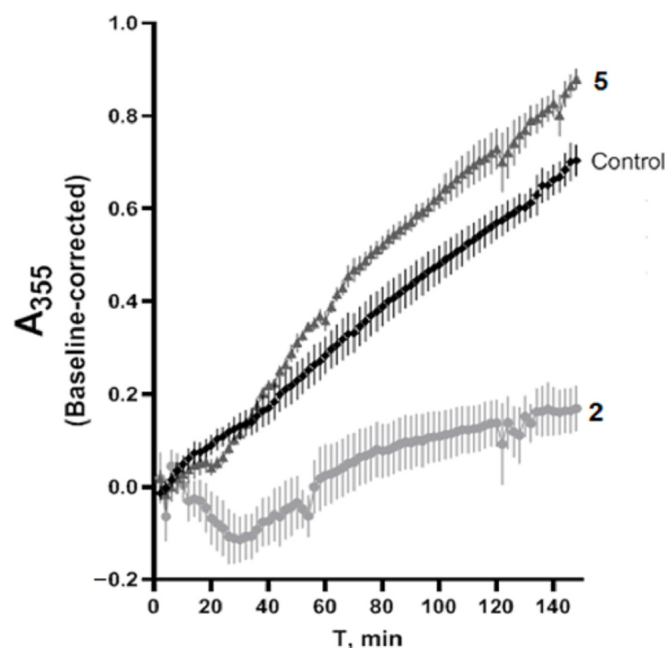


Figure 8. The influence of compounds **2** and **5** (100 μ M) on Tb+MAP polymerization. Results presented as mean \pm SD obtained using at least from three independent experiments.

3. Materials and Methods

3.1. Reagents and Materials

All solvents used were of reagent grade and starting organotin compounds Bu_2SnCl_2 , Ph_2SnCl_2 , Me_2SnBr_2 , Ph_3SnBr (Sigma-Aldrich, Merck KGaA, Darmstadt, Germany, 98%), Trolox (Acros Organics, Geel, Belgium, 97%) were used as supplied. DPPH, neocuproine (2,9-dimethyl-1,10-phenanthroline, 99%) xanthine, EDTA, nitroblue tetrazolium (NBT), xanthine oxidase (0.04 MU) and bovine serum albumin were bought from Sigma-Aldrich.

Infrared absorption spectra were registered using KBr pellets on IR200 (Thermo Nicolet Corporation, Madison, WI, USA) spectrophotometer with Fourier transform. The NMR spectra were obtained using a Bruker Avance-400 (Bruker, Karlsruhe, Germany) spectrometer at different frequencies: 400.1 MHz (^1H), 100.6 MHz (^{13}C) and 149.15 MHz (^{119}Sn) in CDCl_3 and DMSO-d_6 . Orbitrap Elite (Thermo Fisher Scientific, Waltham, MA, USA) mass-spectrometer equipped with an electrospray ionization source (ESI) was used for all high-resolution mass-spectrometry (HRMS) experiments. All compounds dissolved in methanol were directly introduced into the ionization source by means of a syringe pump at 5 $\mu\text{L}/\text{min}$. ESI mass spectra were recorded using positive ionization mode with spray voltage set to 3.4 kV. Xcalibur software (Thermo Xcalibur 3.0.63, Thermo Scientific, Waltham, MA, USA) was used as a system control tool as well as for data collection and data processing. Vaporizer and ion transfer tube temperatures were set to 40 $^\circ\text{C}$ and 275 $^\circ\text{C}$ correspondingly. All spectra were recorded during 30 s in the m/z range 150–1500. Elemental analyses were carried out using a Vario Micro Cube analyzer (Elementar, Berlin, Germany). The determination of the antioxidant activity of the compounds was investigated on an Evolution 300 UV-Visible (Thermo Scientific, Waltham, MA, USA) cuvette spectrophotometer and a microplate (96 wells) spectrophotometer Multiskan Go (Thermo Fisher Sci., Waltham, MA, USA). The MTT test was carried out on a Zenyth200rt (Anthos, Biochrom, Cambridge, UK) multiwell-plate reader.

3.2. Synthesis

Schiff base 2-(-N-3,5-di-*tert*-butyl-4-hydroxyphenyl)iminomethylphenol (**L**), was obtained according to the well-known method [23]. Synthesis of complexes **1**–**5** is demonstrated in Scheme 1.

3.2.1. Synthesis and Characterization of $\text{Me}_2\text{SnBr}_2(\text{L})_2$ (**1**)

A solution of 25 mg (0.07 mmol) Me_2SnBr_2 in 2 mL of CH_2Cl_2 was added to a solution of 50.9 mg (0.148 mmol) of **L** in 3 mL of CH_2Cl_2 . Then the mixture was stirred at 40 $^\circ\text{C}$ for 4 h. The precipitate formed was separated and rinsed with petroleum ether followed by air drying for 24 h. Yield 75 mg (73%); orange-yellow powder; m.p. 135–137 $^\circ\text{C}$. Anal. Calcd for $\text{C}_{44}\text{H}_{60}\text{N}_2\text{O}_4\text{Br}_2\text{Sn}$ (959.47) (%): C, 55.08; H, 6.30; N, 2.92. Found (%): C, 55.32; H, 6.43; N, 2.78. IR (KBr, ν , cm^{-1}): $\nu(\text{OH})$ 3627 (m); $\nu(\text{C-H})$ 2873–2962 (s); $\nu(\text{C=N})$ 1632 (m); 1608; 1486; 1432; 1240; 1157; 766. ^1H NMR (CDCl_3 , 400.1 MHz, δ , ppm): 1.38 (s, 6H, $\text{Sn}(\text{CH}_3)_2$, $^2J_{\text{Sn-H}} = 64$ Hz); 1.49 (s, 36H, $4\text{C}(\text{CH}_3)_3$); 5.29 (s, 2H, 2OH); 6.91 (dd, 2H, Ar, $^3J_{\text{H-H}} = 8$ Hz, $^3J_{\text{H-H}} = 8$ Hz); 7.01 (d, 2H, Ar, $^3J_{\text{H-H}} = 8$ Hz); 7.16 (s, 4H, $2\text{C}_6\text{H}_2$); 7.34–7.41 (m, 4H, Ar), 8.60 (s, 2H, 2CH=N). ^{13}C NMR (CDCl_3 , 100.6 MHz, δ , ppm): 7.52 (Sn-CH_3); 29.80 ($\text{C}(\text{CH}_3)_3$); 34.13 ($\text{C}(\text{CH}_3)_3$); 116.86; 117.48; 118.40; 118.93; 131.55; 132.28; 136.58; 138.71; 146.66; 152.85 (C_{Ar}); 159.34 (CH=N). ^{119}Sn NMR (DMSO-d_6 , 149.15 MHz, δ , ppm): -326.37 .

3.2.2. Synthesis and Characterization of $\text{Bu}_2\text{SnCl}_2(\text{L})_2$ (**2**)

25 mg (0.07 mmol) of Bu_2SnCl_2 was added to a solution of 48 mg (0.16 mmol) of **L** in 7 mL of CH_2Cl_2 . The mixture was stirred at 40 $^\circ\text{C}$ for 1.5 h. The solvent was moved away in a vacuum. The resulting oil was treated with hexane. The precipitate formed was rinsed with hexane followed by air drying for 24 h. To obtain crystals suitable for XRD, the substance was recrystallized from hexane. Yield 120 mg (85%); bright orange crystals; m.p. 118–120 $^\circ\text{C}$. Anal. Calcd for $\text{C}_{50}\text{H}_{72}\text{N}_2\text{O}_4\text{Cl}_2\text{Sn}$ (954.73) (%): C, 62.90; H, 7.60; N, 2.93. Found (%): C, 62.74; H, 7.52; N, 2.65. IR (KBr, ν , cm^{-1}): $\nu(\text{OH})$ 3492 (s); $\nu(\text{C-H})$ 2866–2992

(s); $\nu(\text{C}=\text{N})$ 1641 (s); 1607; 1487; 1432; 1224; 1105; 756. ^1H NMR (CDCl_3 , 400.1 MHz, δ , ppm): 0.94 (t, 6H, $2\text{CH}_2(\text{CH}_2)_2\text{CH}_3$, $^3J_{\text{H-H}} = 8$ Hz); 1.40–1.46 (m, 4H, $2\text{CH}_2(\text{CH}_2)_2\text{CH}_3$); 1.49 (s, 36H, $4\text{C}(\text{CH}_3)_3$); 1.77–1.84 (m, 8H, $2\text{CH}_2(\text{CH}_2)_2\text{CH}_3$); 5.30 (s, 2H, 2OH); 6.92 (dd, 2H, Ar, $^3J_{\text{H-H}} = 8$ Hz, $^3J_{\text{H-H}} = 8$ Hz); 7.01 (d, 2H, Ar, $^3J_{\text{H-H}} = 8$ Hz); 7.16 (s, 4H, $2\text{C}_6\text{H}_2$); 7.34 (dd, 2H, Ar, $^3J_{\text{H-H}} = 8$ Hz, $^3J_{\text{H-H}} = 8$ Hz); 7.39 (d, 2H, Ar, $^3J_{\text{H-H}} = 8$ Hz); 8.60 (s, 2H, $2\text{CH}=\text{N}$). ^{13}C NMR (CDCl_3 , 100.6 MHz, δ , ppm): 13.09 (CH_3CH_2); 25.89 (CH_2); 26.29 (CH_2); 26.47 (CH_2); 29.79 ($\text{C}(\text{CH}_3)_3$); 34.12 ($\text{C}(\text{CH}_3)_3$); 116.79; 117.49; 118.42; 119; 131.47; 132.15; 136.55; 139.54; 152.81; 159.38 (C_{Ar}); 160.81 ($\text{CH}=\text{N}$). ^{119}Sn NMR (CDCl_3 , 149.15 MHz, δ , ppm): 112.52.

3.2.3. Synthesis and Characterization of $\text{Ph}_2\text{SnCl}_2(\text{L})$ (3)

126 mg (0.39 mmol) of **L** was added to a solution of 133 mg (0.39 mmol) of Ph_2SnCl_2 in 8 mL of CH_2Cl_2 . The mixture was stirred at 40 °C for 2 h. The solvent was moved away in a vacuum. The precipitate formed was rinsed with hexane followed by air drying for 24 h.

Yield 258 mg (88%); colour yellow-orange powder; m.p. 76–78 °C. Anal. Calcd for $\text{C}_{33}\text{H}_{37}\text{NO}_2\text{Cl}_2\text{Sn}$ (669.26) (%): C, 59.22; H, 5.57; N, 2.09. Found (%): C, 59.03; H, 5.35; N, 1.85. Selected IR data (KBr, ν , cm^{-1}): $\nu(\text{OH})$ 3615 (s); $\nu(\text{C-H})$ 2873–3052 (s); $\nu(\text{C}=\text{N})$ 1633 (s); 1608; 1484; 1431; 1226; 1151; 731. ^1H NMR (CDCl_3 , 400.1 MHz, δ , ppm): 1.49 (s, 18H, $2\text{C}(\text{CH}_3)_3$); 5.33 (s, 1H, OH); 6.88 (dd, 1H, Ar, $^3J_{\text{H-H}} = 8$ Hz, $^3J_{\text{H-H}} = 8$ Hz); 6.97 (d, 1H, Ar, $^3J_{\text{H-H}} = 8$ Hz); 7.20 (s, 4H, $2\text{C}_6\text{H}_2$); 7.33 (dd, 1H, Ar, $^3J_{\text{H-H}} = 8$ Hz, $^3J_{\text{H-H}} = 8$ Hz); 7.38 (d, 1H, Ar, $^3J_{\text{H-H}} = 8$ Hz); 7.52–7.55 (m, 6H, 2Sn-Ph); 7.72–7.75 (m, 4H, 2Sn-Ph, $^2J_{\text{Sn-H}} = 80$ Hz), 8.57 (s, 1H, $2\text{CH}=\text{N}$). ^{13}C NMR (CDCl_3 , 100.6 MHz, δ , ppm): 29.79 ($\text{C}(\text{CH}_3)_3$); 34.15 ($\text{C}(\text{CH}_3)_3$); 117.41; 118.21; 122.51; 128.13; 129.21; 131.25; 131.77; 132.84; 134.71; 136.70; 137.17; 139.81; 153.02 (C_{Ar}); 159.06 ($\text{CH}=\text{N}$). ^{119}Sn NMR (DMSO-d_6 , 149.15 MHz, δ , ppm): –267.40.

3.2.4. Synthesis and Characterization of $\text{Ph}_2\text{SnCl}_2(\text{L})_2$ (4)

107 mg (0.33 mmol) of **L** and 4 mL of CH_2Cl_2 were added to a solution of 57 mg (0.165 mmol) of Ph_2SnCl_2 in 4 mL of CH_2Cl_2 . The mixture was stirred at 40 °C for 3 h. The solvent was moved away in a vacuum. The precipitate formed was rinsed with hexane followed by air-drying for 24 h.

Yield 164 mg (94%); orange powder; m.p. 87–89 °C. Anal. Calcd for $\text{C}_{54}\text{H}_{64}\text{N}_2\text{O}_4\text{Cl}_2\text{Sn}$ (994.71) (%): C, 65.20; H, 6.49; N, 2.82. Found (%): C, 64.97; H, 6.34; N, 2.76. IR (KBr, ν , cm^{-1}): $\nu(\text{OH})$ 3617 (s); $\nu(\text{C-H})$ 2872–3053 (s); $\nu(\text{C}=\text{N})$ 1634 (s); 1612; 1486; 1432; 1228; 1152; 759. ^1H NMR (CDCl_3 , 400.1 MHz, δ , ppm): 1.49 (s, 36H, $4\text{C}(\text{CH}_3)_3$); 5.31 (s, 2H, 2OH); 6.90 (dd, 2H, Ar, $^3J_{\text{H-H}} = 8$ Hz, $^3J_{\text{H-H}} = 8$ Hz); 7.00 (d, 2H, Ar, $^3J_{\text{H-H}} = 8$ Hz); 7.17 (s, 4H, $2\text{C}_6\text{H}_2$); 7.33 (dd, 2H, Ar, $^3J_{\text{H-H}} = 8$ Hz, $^3J_{\text{H-H}} = 8$ Hz); 7.38 (d, 2H, Ar, $^3J_{\text{H-H}} = 8$ Hz); 7.52–7.55 (m, 6H, 2Sn-Ph); 7.72–7.75 (m, 4H, 2Sn-Ph), 8.57 (s, 2H, $2\text{CH}=\text{N}$). ^{13}C NMR (CDCl_3 , 100.6 MHz, δ , ppm): 29.72 ($\text{C}(\text{CH}_3)_3$); 34.08 ($\text{C}(\text{CH}_3)_3$); 116.51; 117.32; 118.39; 118.95; 126.01; 129.29; 131.41; 131.93; 134.82; 136.96; 139.49; 152.80; 159.29 (C_{Ar}); 160.49 ($\text{CH}=\text{N}$). ^{119}Sn NMR (DMSO-d_6 , 149.15 MHz, δ , ppm): –237.08.

3.2.5. Synthesis and Characterization of $\text{Ph}_3\text{SnBr}(\text{L})_2$ (5)

64 mg (0.15 mmol) of Ph_3SnBr was added to a solution of 50 mg (0.155 mmol) of **L** in 4 mL of CHCl_3 . The mixture was stirred at 40 °C for 1 h. Then it was filtered through a paper filter. The solvent from the filtrate was moved away in a vacuum. The precipitate formed was rinsed with hexane followed by air drying for 24 h.

Yield 85 mg (88%); yellow powder; m.p. 99–101 °C. Anal. Calcd for $\text{C}_{60}\text{H}_{69}\text{N}_2\text{O}_4\text{BrSn}$ (1080.82) (%): C, 66.68; H, 6.43; N, 2.59. Found (%): C, 66.39; H, 6.31; N, 2.42. IR (KBr, ν , cm^{-1}): $\nu(\text{OH})$ 3616 (w); $\nu(\text{C-H})$ 2872–3067 (s); $\nu(\text{C}=\text{N})$ 1635 (w); 1613; 1481; 1431; 1234; 1153; 731. ^1H NMR (CDCl_3 , 400.1 MHz, δ , ppm): 1.49 (s, 36H, $4\text{C}(\text{CH}_3)_3$); 5.29 (s, 2H, 2OH); 6.92 (dd, 2H, Ar, $^3J_{\text{H-H}} = 8$ Hz, $^3J_{\text{H-H}} = 8$ Hz); 7.01 (d, 2H, Ar, $^3J_{\text{H-H}} = 8$ Hz); 7.16 (s, 4H, $2\text{C}_6\text{H}_2$); 7.35 (dd, 2H, Ar, $^3J_{\text{H-H}} = 8$ Hz, $^3J_{\text{H-H}} = 8$ Hz); 7.35–7.41 (m, 4H, 4Ar); 7.46–7.49 (m, 9H, 3Sn-Ph); 7.67–7.70 (m, 6H, 3Sn-Ph), 8.60 (s, 2H, $2\text{CH}=\text{N}$). ^{13}C NMR (CDCl_3 , 100.6 MHz, δ , ppm): 29.79 ($\text{C}(\text{CH}_3)_3$); 34.12 ($\text{C}(\text{CH}_3)_3$); 116.79; 117.50; 118.44; 119.03; 120.68; 128.75;

130.08; 131.45; 132.11; 135.73; 136.41; 136.55; 152.8; 159.41(C_{Ar}); 160.73 (CH=N). ¹¹⁹Sn NMR (DMSO-d₆, 149.15 MHz, δ , ppm): -262.64.

3.3. Crystallographic Data Collection and Structure Determination

All diffraction data were collected on a STOE StadiVari Pilatus 100 K diffractometer (Stoe&Cie, Darmstadt, Germany) [$\lambda(\text{MoK}\alpha) = 0.71073 \text{ \AA}$, $\lambda(\text{CuK}\alpha) = 1.5418 \text{ \AA}$, ω -scans] at 293 K [24]. The primary processing of the experimental data array was performed using the WinGX program package [25]. The structures were solved by direct methods and refined by full-matrix least-squares procedures on F² using SHELXL97 [26]. All non-hydrogen atoms were refined anisotropically, and hydrogen atoms were located at calculated positions and refined via the 'riding model'. Crystal data and structure refinement parameters are listed in Table 1. CCDC2205597 (1), 2205598 (2) contain the supplementary crystallographic data for this paper. The structures of complexes were drawn using the MERCURY CSD 3.1 program [27].

3.4. CUPRAC Assay (Cu²⁺ Reducing)

The method proposed by Apak et al. was used with slight modification [14]. For this reason, 0.05 mL of CuCl₂ solution (0.01 M), 0.05 mL of methanol neocuproine solution (7.5 mM) and 0.25 mL of ammonium acetate buffer solution (1 M) were added to a test tube, followed by mixing with different concentrations of tested compounds (10–100 μM). The mixtures were kept at room temperature. Absorbance was measured at 450 nm on Multiskan Go microplate spectrophotometer (Thermo Fisher Sci., Waltham, MA, USA) against a reagent blank 35 min later. The increase of reaction mixture absorbance in comparison with control indicates the reduction capability of the test compound. Results were presented in Trolox-equivalents. TEAC CUPRAC values were obtained graphically using absorbance data and a linear calibration curve plotted as absorbance vs. Trolox concentration.

3.5. DPPH Radical Scavenging Activity

The free radical scavenging activity was evaluated using the stable radical DPPH, according to the method described by Brand-Williams et al. with a slight modification [15]. For each compound, a 1:1 ratio expressed as moles of compound per mole of DPPH radical was tested. A 1 mL sample of the compound solution in ethanol was added to 1 mL of DPPH solution in ethanol so that the initial DPPH concentration in the cuvettes was 0.1 mM. The samples were incubated for 1 h at 20 °C in ethanol and the decrease in the absorbance values of the DPPH solution was measured at λ_{max} 517 nm on the Evolution 300 UV-Visible (Thermo Scientific) cuvette spectrophotometer. Results were expressed as scavenging activity calculated as follows:

$$\text{Scavenging activity, \%} = [(A_0 - A_1)/A_0] \times 100$$

The concentration of compound needed to decrease 50% of the initial DPPH concentration (EC₅₀) is a parameter widely used to measure the antioxidant effect. For determination of the EC₅₀ the values of DPPH decrease after 1 h were used. The EC₅₀ values were calculated graphically by plotting scavenging activity against compound concentration. Different sample concentrations (0.01, 0.02, 0.04, 0.06, 0.08 and 0.1 mM) were used in order to obtain kinetic curves and to calculate the EC₅₀ values.

3.6. Lipoygenase Inhibition Assessment

Lipoygenase type 1B (LOX-1B) from Glycine max (soybean), boric acid, linoleic acid, ammonium acetate, CuCl₂, and ethanol (96%) were purchased from Sigma-Aldrich and were used with no further purification. LOX-1B inhibition activity was determined spectrophotometrically [16] by measuring the increase in absorbance at 234 nm for the oxidation of linoleic acid on the Multiskan Go microplate spectrophotometer (Thermo Scientific). The reaction mixture contained 3 μL of test compounds dissolved in DMSO at

initial concentrations of 0.05–2 mM (final concentrations 0.8, 3.3, 8.3, 16.6, 33.3 μM); 100 μL of 0.3 mM linoleic acid; 30 μL of borate buffer (pH = 9.0) and 17 μL of lipoxygenase solution in borate buffer. The total sample volume was 150 μL . The total cell volume used for UV-Vis measurements is 300 μL . The increase in absorbance was recorded every 10 s during 10 min under a controlled temperature 25 °C. All experiments were performed in triplicate.

The degree of LOX-1B activity (I %) in the presence of the complexes (Table 5) was calculated according to the following [5]:

$$I, \% = (\nu_o \text{ in the presence of inhibitor} / \nu_o \text{ in the absence of inhibitor}) \times 100,$$

where ν_o is the initial rate. The value of the initial rate (ν_o , $\mu\text{M min}^{-1}$) was calculated according to the formula:

$$\nu_o = \Delta C / \Delta t = \Delta A / \Delta t \epsilon = \text{tg}\alpha / \Delta t \epsilon,$$

where C is the concentration of product (hydroperoxy-linoleic acid), t is the reaction time, ϵ is the molar absorbance coefficient of hydroperoxy-linoleic acid and $\text{tg}\alpha$ is the slope of the kinetic curve plotted as absorbance vs. time.

3.7. Antiproliferative Activity [28]

The human HCT116 colorectal carcinoma, A549 non-small cell lung carcinoma, MCF7 breast adenocarcinoma cell lines and WI-38 diploid human cell line composed of fibroblasts were obtained from the European collection of authenticated cell cultures (ECACC; Salisbury, UK) All cells were grown in a DMEM medium (Gibco™, Ireland) supplemented with 10% fetal bovine serum (Gibco™, Brazil). The cells were cultured in an incubator at 37 °C in a humidified 5% CO₂ atmosphere and were sub-cultured 2 times a week. The effect of the investigated compounds on cell proliferation was evaluated using a common MTT assay. The cells were seeded in 96-well tissue culture plates («TPP», Trasadingen, Switzerland) at 7×10^3 cells/well in 100 μL of the medium. After overnight incubation at 37 °C, the cells were treated with the tested compounds in the concentration range of 0 to 100 μM . Cisplatin was used as a standard. After 72 h of treatment, the solution was removed, and a freshly diluted MTT solution (100 μL , 0.5 mg/mL in cell medium) was added to the wells, and the plates were further incubated for 50 min. Subsequently, the medium was removed, and the formazan product was dissolved in 100 μL of DMSO. The number of living cells in each well was evaluated by measuring the absorbance at 570 nm using the «Zenith 200 rt» microplate reader (Biochrom, Cambridge, UK) The meanings of 50% inhibition concentration (IC₅₀) with standard deviation were calculated using GraphPad Prism Version 5.03 for Windows.

3.8. Cell Death and Cell Cycle Analysis

HCT-116 cells (colon carcinoma) (1×10^6) were seeded in a 6-well plate and incubated with **2**, **5** and cisplatin (values based on MTT assay) at $2 \times \text{IC}_{50}$ for 24 and 48 h. After incubation, the cells were harvested by trypsinization, precipitated by centrifugation (3500 rpm), washed with cold PBS and recentrifuged. Aliquots of cells were processed as recommended in the Muse AnnexinV&Dead Cell Kit. The results were recorded on a Muse Cell Analyzer flow cytometer (Luminex corp., Austin, TX, USA) [20].

For the cell cycle analysis, HCT-116 cells (1×10^6) were seeded in a six-well plate and were incubated for 24 h and then the medium was treated with compounds at the concentrations IC₅₀ and incubated for 24 h. After incubation, the cells were harvested by trypsinization and precipitated by centrifugation (3500 rpm). After precipitation, the supernatant was removed, washed with PBS, centrifuged, fixed with 70% ethanol and incubated for at least 3 h at –20 °C. After incubation, 200 μL of the cell suspension was collected, centrifuged, the supernatant was removed, and washed with 200 μL of PBS. Then, the cells were stained 200 μL of the Muse Cell Cycle Reagent and incubated for 30 min at r.t.

in the dark. Cell cycle analysis was performed using a Muse Cell Analyzer flow cytometer (Merck, Rahway, NJ, USA).

3.9. Tubulin Polymerization

Evaluation of the effect of compounds on tubulin polymerization performed according to [29]. A crude fraction of tubulin and microtubule-associated proteins (Tb+MAP) was isolated from mouse brain tissue by a polymerization–depolymerization method [30].

The procedure of mouse euthanasia using cervical dislocation for Tb+MAP preparation is in compliance with the Guidelines for Animal Experiments, which were approved by the local bioethics committee of the IPAC RAS. The freshly dissected brain was immediately placed on ice, cleared of meninges and surface blood vessels, and washed with cold buffer A (50 mM Tris-HCl, pH 6.9 at 4 °C, 2 mM EGTA). The extracted brain tissue was homogenized under ice cooling in the same buffer using a Potter S homogenizer (Sartorius, Göttingen, Germany). The resulting homogenate was centrifuged at $10,000\times g$ for 30 min on an Avanti 25 centrifuge (Beckman, Brea, CA, USA) using a JA-14 rotor for the precipitation of non-ruptured cells. The precipitate was discarded, and the supernatant was again centrifuged at $100,000\times g$ for 60 min at 4 °C on an Optima MAX XP centrifuge (Beckman, Brea, CA, USA) using a MLA-50 rotor. The precipitate was again discarded. The protein concentration in the supernatant was determined by the Bradford assay using the Bio-Rad Protein Assay kit (Bio-Rad, Hercules, CA, USA) according to the manufacturer's instructions. The resulting supernatant was a cytosolic fraction enriched in microtubular proteins (Tb and MAP). The Tb+MAP preparation was centrifuged at $5000\times g$ for 10 min at 4 °C immediately before polymerization in order to remove denatured and aggregated protein molecules by precipitation. The Tb+MAP polymerization was performed at 37 °C in buffer A in the presence of 0.1 mM GTP after the addition of 100 M of test compound or the same volume of vehicle (DMSO). The protein concentration in the sample was 0.2 mg/mL. The polymerization kinetics was monitored on a Victor 3 or EnVision microplate reader (Perkin Elmer, Waltham, MA, USA) at 355 nm.

4. Conclusions

Novel polyfunctional organotin complexes 1–5 based on a Schiff base containing an antioxidant 2,6-di-*tert*-butylphenol moiety were obtained and characterized. Using XRD method, the structures of initial ligand L and compound 2 were defined. In complex 2 the ligand is coordinated by O atom to the Sn center and distorted octahedron geometry was observed. In addition, a proton transfer from the oxygen atom to the nitrogen atom in the ligand part was revealed for complex 2.

Complexes 1 and 5 demonstrated high antioxidant activity in CUPRAC- and DPPH-methods due to their ability to be involved in one-electron and hydrogen atom transfer. The antioxidant activity was also explored in the enzymatic oxidation of linoleic acid by lipoxygenase (LOX 1-B) *in vitro*. Only compound 4 was found to be a moderate inhibitor of LOX 1-B.

The antiproliferative activity of complexes 1–5 was studied *in vitro* on HCT-116, MCF-7, A-549 and WI-38 cancer cell lines in the MTT test. It was established that dibutyl- and triphenyltin complexes 2 and 5 were the most active. Apoptosis and the cell cycle analysis were investigated by flow cytometry on HCT-116 cell line for these compounds after 24 and 48 h. Complex 2 was found to be the most active compound inducing apoptosis. Moreover, compounds 2 and 5 blocked proliferation in the G2/M phase of the cell cycle. The mechanism of antiproliferative activity of compounds 2 and 5 may be also connected with their influence on Tb+MAP polymerization.

Thus, the obtained compounds demonstrate high biological activity, which makes them promising for further research as potential anti-tumor agents with possible combined actions.

Supplementary Materials: The following supporting information can be downloaded at: <https://www.mdpi.com/article/10.3390/ijms24032024/s1>.

Author Contributions: Conceptualization, T.A.A. and A.A.N.; Funding acquisition, T.A.A.; Investigation Y.A.G., D.B.S., M.A.V., D.M.M., V.A.T., Y.F.O., E.F.S., P.N.S. and A.A.N.; Supervision, E.R.M.; Writing—original draft preparation, T.A.A., Y.A.G., D.B.S., D.M.M. and E.R.M. All authors have read and agreed to the published version of the manuscript.

Funding: This research was funded by financial support of scholarship of the President of the Russian Federation for young scientists and graduate students (Grants Council of the President of the Russian Federation for state support of young Russian scientists and state support of the leading scientific schools of the Russian Federation, No. SP-1641.2021.4).

Institutional Review Board Statement: Not applicable.

Informed Consent Statement: Not applicable.

Data Availability Statement: Copies of ^1H , ^{13}C , ^{119}Sn NMR, ECI-MS spectra and structure files of the synthesized compounds are presented in the Supplementary Materials.

Acknowledgments: The authors are thankful to Alexander Makarov for providing the Orbitrap Elite mass spectrometer for this work. We also acknowledge the use of a STOE STADIVARI single-crystal X-ray diffractometer purchased under the Lomonosov MSU Program of Development and the “Centre for Collective Use of IPAC RAS” (IPAC research topic FFSN-2021-0005) for use of equipment for biological assay of tubulin polymerization.

Conflicts of Interest: The authors declare no conflict of interest.

References

1. Milaeva, E.R.; Tyurin, V.Y. Hybrid metal complexes with opposed biological modes of action—Promising selective drug candidates. *Pure Appl. Chem.* **2017**, *89*, 1065–1088. [[CrossRef](#)]
2. Milaeva, E.R.; Shpakovsky, D.B.; Gracheva, Y.A.; Antonenko, T.A.; Ksenofontova, T.D.; Nikitin, E.A.; Berseneva, D.A. Novel selective anticancer agents based on Sn and Au complexes. Mini-review. *Pure Appl. Chem.* **2020**, *92*, 1201–1216. [[CrossRef](#)]
3. Antonenko, T.A.; Gracheva, Y.A.; Shpakovsky, D.B.; Vorobyev, M.A.; Tafenko, V.A.; Mazur, D.M.; Milaeva, E.R. Cytotoxic activity of organotin compounds containing non-steroidal anti-inflammatory drugs. *J. Organomet. Chem.* **2022**, *960*, 122191. [[CrossRef](#)]
4. Adeyemi, J.O.; Onwudiwe, D.C. Organotin(IV) Dithiocarbamate Complexes: Chemistry and Biological Activity. *Molecules* **2018**, *23*, 2571. [[CrossRef](#)]
5. Xanthopoulou, M.N.; Hadjikakou, S.K.; Hadjiliadis, N.; Milaeva, E.R.; Gracheva, J.A.; Tyurin, V.Y.; Kourkoumelis, N.; Christoforidis, K.C.; Metsios, A.K.; Karkabounas, S.; et al. Biological studies of new organotin(IV) complexes of thioamide ligands. *Eur. J. Med. Chem.* **2008**, *43*, 327–335. [[CrossRef](#)]
6. Dave, S.; Bansal, N. Analgesic And Anti-Inflammatory Activities Of Schiff Base Metal Complexes—A Review. *Int. J. Basic App. Chem. Sci.* **2013**, *3*, 31–40.
7. Elshafie, H.S.; Sadeek, S.A.; Camele, I.; Mohamed, A.A. Biochemical Characterization of New Gemifloxacin Schiff Base (GMFX-ophdn) Metal Complexes and Evaluation of Their Antimicrobial Activity against Some Phyto- or Human Pathogens. *Int. J. Mol. Sci.* **2022**, *23*, 2110. [[CrossRef](#)]
8. Mohamed, A.A.; Ahmed, F.M.; Zordok, W.A.; El-Shwiniy, W.H.; Sadeek, S.A.; Elshafie, H.S. Novel Enrofloxacin Schiff Base Metal Complexes: Synthesis, Spectroscopic Characterization, Computational Simulation and Antimicrobial Investigation against Some Food and Phyto-Pathogens. *Inorganics* **2022**, *10*, 177. [[CrossRef](#)]
9. El-Attar, M.S.; Ahmed, F.M.; Sadeek, S.A.; Mohamed, S.F.; Zordok, W.A.; El-Shwiniy, W.H. Characterization, DFT, and antimicrobial evaluation of some new N2O2 tetradentate Schiff base metal complexes. *Appl. Organomet. Chem.* **2022**, *36*, e6826. [[CrossRef](#)]
10. Gielen, M.; Tiekink, E.R.T. (Eds.) *Metallotherapeutic Drugs and Metal-Based Diagnostic Agents: The Use of Metals in Medicine*; Wiley: Chichester, UK, 2008; p. 656.
11. Shpakovsky, D.B.; Banti, C.N.; Mukhatova, E.M.; Gracheva, Y.A.; Osipova, V.P.; Berberova, N.T.; Albov, D.V.; Antonenko, T.A.; Aslanov, L.A.; Milaeva, E.R.; et al. Synthesis, antiradical activity and in vitro cytotoxicity of novel organotin complexes based on 2,6-di-tert-butyl-4-mercaptophenol. *Dalton Trans.* **2014**, *43*, 6880–6890. [[CrossRef](#)]
12. Kolyada, M.N.; Osipova, V.P.; Berberova, N.T.; Shpakovsky, D.B.; Milaeva, E.R. Porphyrins with Phenolic Fragments at the Periphery of the Macrocyclic as Perspective Antioxidants, Cytoprotectors and Heavy Metal Scavengers. *Chem. Heterocycl. Compd.* **2021**, *57*, 875–888. [[CrossRef](#)]
13. Antonenko, T.A.; Shpakovsky, D.B.; Vorobyov, M.A.; Gracheva, Y.A.; Kharitonashvili, E.V.; Dubova, L.G.; Shevtsova, E.F.; Tafenko, V.A.; Aslanov, L.A.; Iksanova, A.G.; et al. Antioxidative vs cytotoxic activities of organotin complexes bearing 2,6-di-tert-butylphenol moieties. *Appl. Organomet. Chem.* **2018**, *32*, e4381. [[CrossRef](#)]

14. Apak, R.; Güçlü, K.; Özyürek, M.; Karademir, S.E. Novel Total Antioxidant Capacity Index for Dietary Polyphenols and Vitamins C and E, Using Their Cupric Ion Reducing Capability in the Presence of Neocuproine: CUPRAC Method. *J. Agric. Food. Chem.* **2004**, *52*, 7970–7981. [[CrossRef](#)]
15. Brand-Williams, W.; Cuvelier, M.E.; Berset, C. Use of a free radical method to evaluate antioxidant activity. *LWT Food Sci. Technol.* **1995**, *28*, 25–30. [[CrossRef](#)]
16. Ozturk, I.; Filimonova, S.; Hadjidakou, S.K.; Kourkoumelis, N.; Dokorou, V.; Manos, M.J.; Tasiopoulos, A.J.; Barsan, M.M.; Butler, I.S.; Milaeva, E.R.; et al. Structural Motifs and Biological Studies of New Antimony(III) Iodide Complexes with Thiones. *Inorg. Chem.* **2010**, *49*, 488–501. [[CrossRef](#)] [[PubMed](#)]
17. Nikš, M.; Otto, M. Towards an optimized MTT assay. *J. Immunol. Methods* **1990**, *130*, 149–151. [[CrossRef](#)]
18. Hadjidakou, S.K.; Hadjiliadis, N. Antiproliferative and anti-tumor activity of organotin compounds. *Coord. Chem. Rev.* **2009**, *253*, 235–249. [[CrossRef](#)]
19. Banti, C.N.; Hadjidakou, S.K.; Sismanoglu, T.; Hadjiliadis, N. Anti-proliferative and antitumor activity of organotin(IV) compounds. An overview of the last decade and future perspectives. *J. Inorg. Biochem.* **2019**, *194*, 114–152. [[CrossRef](#)]
20. Vermes, I.; Haanen, C.; Steffens-Nakken, H.; Reutellingsperger, C. A novel assay for apoptosis Flow cytometric detection of phosphatidylserine expression on early apoptotic cells using fluorescein labelled Annexin V. *J. Immunol. Methods* **1995**, *184*, 39–51. [[CrossRef](#)]
21. Milaeva, E.R.; Shpakovsky, D.B.; Gracheva, Y.A.; Antonenko, T.A.; Osolodkin, D.I.; Palyulin, V.A.; Shevtsov, P.N.; Neganova, M.E.; Vinogradova, D.V.; Shevtsova, E.F. Some insight into the mode of cytotoxic action of organotin compounds with protective 2,6-di-tert-butylphenol fragments. *J. Organomet. Chem.* **2015**, *782*, 96–102. [[CrossRef](#)]
22. Cheng, Z.; Lu, X.; Feng, B. A review of research progress of antitumor drugs based on tubulin targets. *Transl. Cancer Res.* **2020**, *9*, 4020–4027. [[CrossRef](#)] [[PubMed](#)]
23. Medzhidov, A.A.; Kasumov, V.T.; Mamedov, K.S. Synthesis and study of chelate compounds of metals containing spatially hindered phenol. *Koord. Khim.* **1981**, *7*, 66–72.
24. Stoe&Cie. X-AREA, X-RED32; Stoe&Cie: Darmstadt, Germany, 2012.
25. Farrugia, L. WinGX and ORTEP for Windows: An update. *J. Appl. Crystallogr.* **2012**, *45*, 849–854. [[CrossRef](#)]
26. Sheldrick, G. A short history of SHELX. *Acta Crystallogr. Sect. A Found. Crystallogr.* **2008**, *64*, 112–122. [[CrossRef](#)] [[PubMed](#)]
27. Macrae, C.F.; Edgington, P.R.; McCabe, P.; Pidcock, E.; Shields, G.P.; Taylor, R.; Towler, M.; van de Streek, J. Mercury: Visualization and analysis of crystal structures. *J. Appl. Crystallogr.* **2006**, *39*, 453–457. [[CrossRef](#)]
28. Shutkov, I.A.; Okulova, Y.N.; Tyurin, V.Y.; Sokolova, E.V.; Babkov, D.A.; Spasov, A.A.; Gracheva, Y.A.; Schmidt, C.; Kirsanov, K.I.; Shtil, A.A.; et al. Ru(III) Complexes with Lonidamine-Modified Ligands. *Int. J. Mol. Sci.* **2021**, *22*, 13468. [[CrossRef](#)]
29. Bachurin, S.O.; Makhaeva, G.F.; Shevtsova, E.F.; Aksinenko, A.Y.; Grigoriev, V.V.; Shevtsov, P.N.; Goreva, T.V.; Epishina, T.A.; Kovaleva, N.V.; Pushkareva, E.A.; et al. Conjugation of Aminoadamantane and γ -Carboline Pharmacophores Gives Rise to Unexpected Properties of Multifunctional Ligands. *Molecules* **2021**, *26*, 5527. [[CrossRef](#)]
30. Shelanski, M.L.; Gaskin, F.; Cantor, C.R. Microtubule assembly in the absence of added nucleotides. *Proc. Natl. Acad. Sci. USA* **1973**, *70*, 765–768. [[CrossRef](#)]

Disclaimer/Publisher’s Note: The statements, opinions and data contained in all publications are solely those of the individual author(s) and contributor(s) and not of MDPI and/or the editor(s). MDPI and/or the editor(s) disclaim responsibility for any injury to people or property resulting from any ideas, methods, instructions or products referred to in the content.